Journal of Physics: Conference Series **543** (2014) 012013 doi:10.1088/1742-6596/543/1/012013

Polarized target options for deuteron tensor structure function studies

O A Rondon-Aramayo
Institute for Nuclear and Particle Physics, U. of Virginia, Charlottesville, VA
E-mail: or@virginia.edu

Abstract. Studies of spin-dependent observables generally rely on calculating the difference between scattering yields for opposite spin states of the beam helicity or the target polarization or both. While the beam helicity can be changed at rates of up to many times per second, target polarization flips involve times on the order of hours or longer. To measure observables that depend only on the differences for opposite target polarizations with minimal systematic effects caused by changes in the beam, target, and detector systems, special methods need to be followed. One option is to use targets which have two or more sections in the beam path, each with materials polarized independently. While this approach does not remove all sources of systematic effects, it can be combined with frequent alternation of spin states to improve the control of time dependent and configuration uncertainties.

1. Introduction

A general expression for spin dependent electromagnetic scattering cross-sections looks like [1, 2]

$$\sigma = \sigma^U(1 + h\cancel{A^h} + P_V A_V + P_T A_T + h(P_V A_V^h + P_T A_T^h)) \quad (1)$$

where σ^U is the spin independent cross section, h is the beam helicity, P_V and P_T are the vector and tensor target polarizations, respectively, A_V and A_T are single spin vector and tensor target asymmetries and A_V^h and A_T^h are the corresponding double spin ones. The out-of-plane beam A_h is crossed out because it is absent in inclusive scattering. Moreover, A_T and A_T^h are zero for spin $< 1\hbar$.

The target asymmetries depend on opposite target polarizations, which are hard to flip, unlike the beam helicity. The experimenter is then faced with two options to flip $P_{t(arget)}$:

- use a single cell target with periods of alternating P_t
- use a target with multiple cells, each with independent P_t (which could also be zero.)

An example of such observable is the deuteron tensor structure function (SF) b_1^d. The cross section for unpolarized electrons scattering on longitudinally polarized deuterons [3] as a function of the Bjorken scaling variable x and the four-momentum transfer Q^2 is

$$\sigma^{\parallel}(x, Q^2) = Kx(F_1^d(x, Q^2) - \frac{P_{zz}}{3} b_1^d(x, Q^2)) \quad (2)$$

where $K(y, E, Q^2)$ is a kinematical factor which depends on the beam energy E and the fractional energy transfer $y = \nu/E$, $\nu = E - E'$ is the difference between the beam and the scattered energy.

For $P_{zz} = 0$ one obtains the unpolarized cross section $\sigma^U = KxF_1^d$. The tensor SF can then be isolated from the cross section difference

$$\sigma^U - \sigma^{\parallel} = Kx\frac{P_{zz}}{3}b_1^d.$$

b_1 can be measured by taking data simultaneously on two (or more) unpolarized and polarized in-line cells: the yields from all cells share the beam charge and detector efficiency. Moreover, for multiple data taking periods with alternating cell polarizations, one can form yield differences for both beam upstream–downstream cells, and same cell differences for different polarization periods.

2. Multiple cell polarized targets

The concept of multiple cell polarized targets is not novel. It was introduced introduced by the EMC experiment (CERN NA2') to deal with the single sign of the polarization of muon beams (always negative). It consisted of upstream and downstream cells [4], with separate microwave feeds, as indicated on Fig. 1. A similar configuration was used in subsequent targets, like those used in SMC [5], see Fig. 2, and COMPASS [6], see Fig. 3.

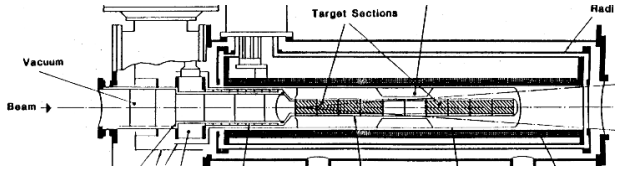

Figure 1. EMC dual cell target.

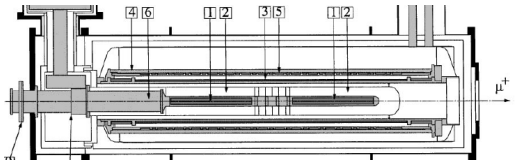

Figure 2. SMC dual cell target.

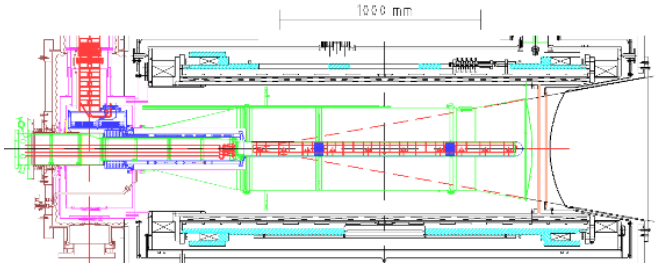

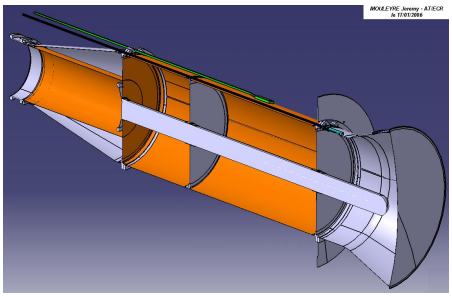

Figure 3. Left: COMPASS triple cell target. Right: Cutaway view of COMPASS target cells [7].

Multiple cell targets have favorable and unfavorable features. Among the pros one can count

- can compensate for few or no polarization reversals by taking data simultaneously on two or more polarization states
- use favorable cylindrical symmetry for simple, intense solenoidal magnetic fields ≥ 6.5T
- increased data rate, allowing lower beam currents than single cell systems, which results in fewer anneals and material changes
- reduced or eliminated time dependent systematic effects.

The cons include

- more complicated systems for refrigeration, microwaves feeding and isolation

- increased radiation thickness increases external radiative corrections
- event loss from acceptance matching cuts
- cell dependent packing fractions.

3. A more detailed look

In order to evaluate the possibility of using multiple cell targets in experiments at JLab, a more detailed look at their features is needed.

The most important component of multiple cell targets are the coils. Their geometry and configuration determine critical aspects, such as angular acceptance and achievable polarization levels. The CERN targets used a solenoidal geometry with a main coil with a length L to radius R aspect ratio $L/R = 20/3.3$. This ratio determines in part the angular apertures for scattered particles and the need for additional trim and compensation coils to achieve the field homogeneity required for dynamic nuclear polarization - DNP, over a region of significant size where the polarizable material is located.

The solenoid magnet of the COMPASS target used coils first built by Saclay [6], shown in Fig. 3, which were later upgraded to ones built by Oxford Instruments [8], shown in Fig. 4. The magnet in both cases consisted of a 2.7 T solenoid plus 0.5 T dipole for transverse field. Fig. 5 illustrates the coil configuration for the Saclay magnet. The field had a better than 10^{-4} uniformity and it initially accommodated two 30 mm diameter cylindrical cells 60 cm long each with a 5 cm spacing in between. The cells were later upgraded to 40 mm diameter ones, with three sections: upstream + downstream, 30 + 30 cm, and a central 60 cm long one, shown on Fig. 3.

With the Oxford magnet the system had a $\pm 14°$ downstream acceptance, while the Saclay magnet allowed only ± 75 mr, or less than 5°.

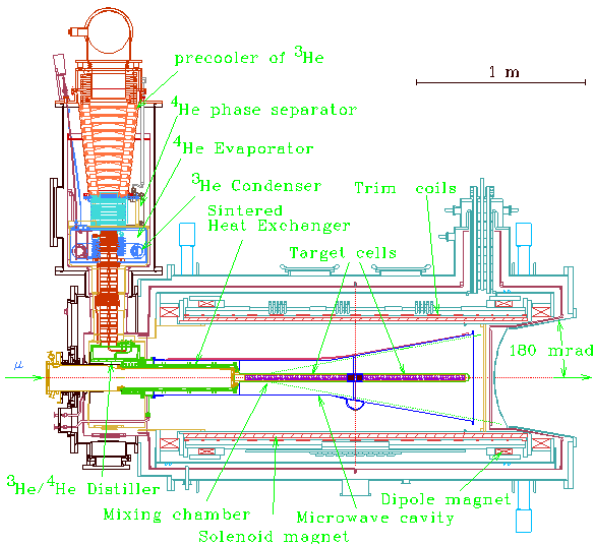

Figure 4. Diagram of the COMPASS target with the Oxford Instruments magnet [8].

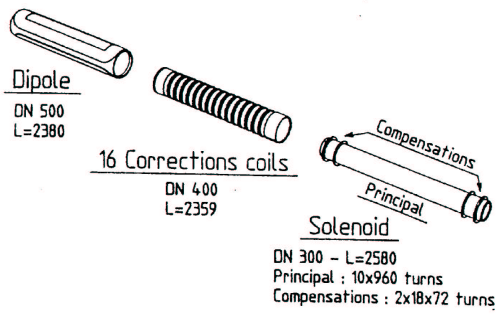

Figure 5. Exploded view diagram of the Saclay coils [9].

Given the excellent characteristics of the COMPASS Oxford magnet, it serves as a guide for designing a similar system for JLab polarized target experiments that would benefit from data simultaneously taken on multiple cells. Some criteria on magnet design for a multi-cell target for high intensity electron beams would be

- Solenoid for longitudinal field, including trim and compensation coils to achieve equal or better than 10^{-4} uniformity over the length of the cups. This could be done for JLab with a 1/5 scale copy of the Oxford magnet, with a slightly better aspect ratio of $L/R = 20/3$
- A uniform region of ±6.5 cm, or a tenth of COMPASS's ±65 cm, which would help in reducing the number of required correction coils.
- An optional dipole for transverse field.

For a 1/5 scale coil relative to the COMPASS magnet, the ratio BL(JLab)/BL(COMPASS) = 6.75 T × 40 cm/(2.7 T × 200 cm) = 0.5 means that the NI ampere turns for a 6.75 T JLab solenoid would be 1/2 that of the COMPASS coil.

An example of a possible coil design is illustrated in Fig. 6, consisting of a 40 cm long, 6 cm radius solenoid. The uniform field region would extend over ±6.5 or 7 cm, to fit two cells, each about 4 cm long, spaced by up to 5 cm to obtain clean vertex separations. The minimum downstream acceptances for this setup would be about 10.7° for the 4 cm cups spaced 5 cm. The acceptance could exceed 11.8° for 3 cm cups spaced 2 cm displaced downstream along the coil center. The optimal configuration would be determined after detailed modeling of coil and cell characteristics.

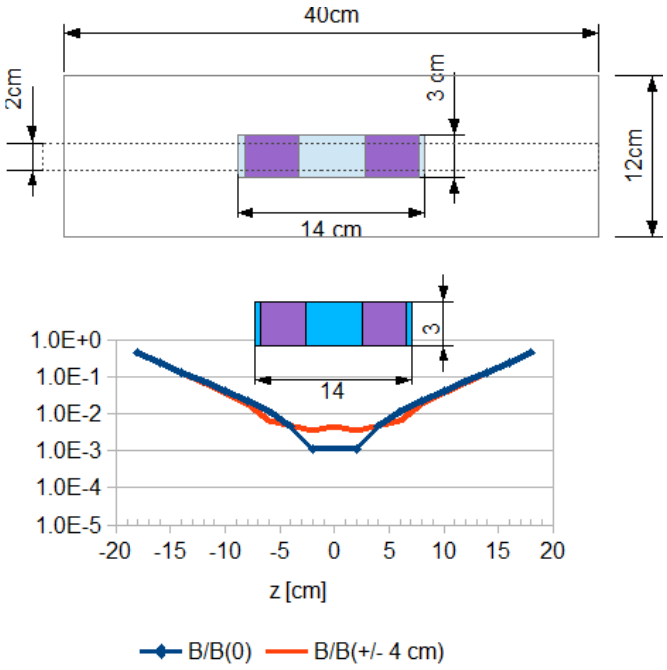

Figure 6. Possible solenoid coil design for JLab. The dashed lines represent the 1 cm radius envelope of the rastered beam. The curves represent the ratio of the pure solenoidal field along the axis (blue online, dark curve with diamonds) to the field at the center, and at ±4 cm from the center (red online, light smooth curve).

4. Using multiple cell targets

Special considerations need to be applied when designing experiments and analyzing data taken with multiple cell targets. The most important one probably is to have good vertex reconstruction to identify data from individual cells. Clean separation with small loss of events from the ends of the cells is a must. This can be achieved by allowing adequate spacing between cells, at the possible price of complicating the matching of acceptances. Fig. 7 illustrates the vertex separation after cuts obtained with the triple cell COMPASS target [10].

For the case of the JLab spectrometers, figure 8 top panel shows the results of simulated vertex reconstruction with the Hall C High Momentum spectrometer - HMS at 14°, for an arrangement of two 4 cm long cells filled with solid ammonia and liquid He, located upstream

and downstream of the target center and separated by 5 cm filled with LHe only, with additional 0.5 cm LHe at their extreme ends, like the example shown on Fig. 6. The bottom panel of the same figure shows the simulation for the Super HMS at 12°, this time with no LHe between the cells, but 0.5 cm LHe at all four ends. 11 GeV electrons were incident in both cases. No cuts on the scattering polar and azimuthal angles were applied. The upstream and downstream distributions can be matched to better than 1% applying angle acceptance cuts, with a tolerable yield loss of about 60%. The simulated data were prepared by Narbe Kalantarians.

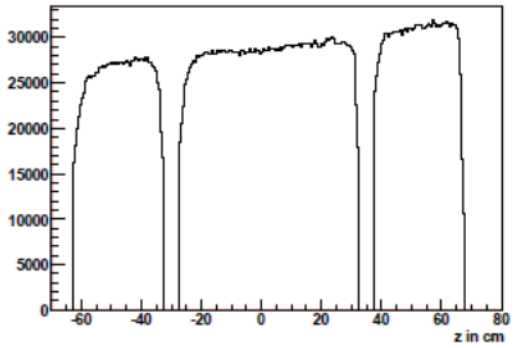

Figure 7. Vertex reconstruction, after cuts, of data taken with the triple cell COMPASS target.

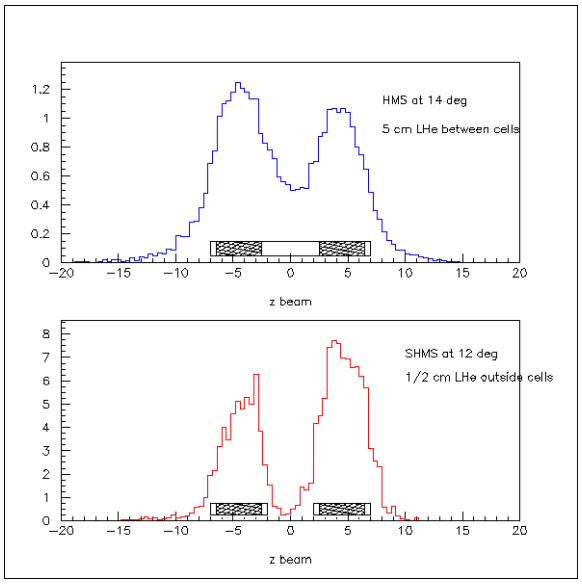

Figure 8. Top: vertex reconstruction of simulated HMS data. Bottom: SHMS vertex reconstruction.

As mentioned above, many types of yield differences can be formed with multi-cell target configurations, which are not possible with single cell systems. Moreover, each type is subjected to different systematic effects.

Time dependent effects, such as changing beam charge calibrations and detector efficiency, which affect single cell systems, aren't present for multiple cell ones. On the other hand, multi-cell setups have to deal with cell dependent acceptances $\mathcal{A} = \Delta E' \Delta\Omega$. In both cases, the total amount of polarizable material, or packing fraction, is also a source of systematic differences, time dependent ones for both cases and cell dependent ones for multiple cells.

For multiple cells it is important to optimize the length vs the size of the radiative corrections by balancing faster counting vs systematic errors. For example, for 3 + 3 cm cells with 60% packing fractions, each $4.6\%X_0$ long, the increase in external radiative corrections could be more than compensated by the doubling of the total Born rate compared with the single cups used in past polarized target experiments in JLab's Hall C, such as G_E^n (E93-028), RSS (E01-006) and SANE (E07-003).

But the main advantage of multi-cell targets is that many types of differences between subsets of data can be formed. Examples of possible differences are shown on the table of Fig. 9. COMPASS used a similar labeling scheme for their triple cell, even subdividing the large central cell into two virtual subcells [11].

	Cell		Differences		Changes
Period	U	D	Different cells	Same cell	
1	U_0	D_p	$\Delta_1^{\,d} = U_{01} - D_{p1}$		$\mathcal{A}_{U,D}$, $pf_{U,D}$
2	U_p	D_0	$\Delta_2^{\,d} = U_{p2} - D_{02}$		
				$\Delta_U^{\,s} = U_{01} - U_{p2}$, $\Delta_D^{\,s} = D_{p1} - D_{02}$	$Q_{1\text{-}2}$, $\varepsilon_{1\text{-}2}$, $pf_{1,2}(U)$,$pf_{1,2}(D)$
3	U_p	D_0			
4	U_0	D_p			
			$\Delta_U^{\,4} = U_{01} + U_{04} - (U_{p2} + U_{p3})$, $\Delta_D^{\,4} = D_{p1} + D_{p4} - (D_{02} + D_{03})$		

Figure 9. Some types of differences among data subsets that can be formed with multiple cell setups. U and D refer to beam upstream or downstream. The subscripts "p" and "0" indicate the polarization state of the cell in a given period ("p"olarized or unpolarized - "0"). $\mathcal{A}$ is the acceptance, p_f is the packing fraction, Q is the beam charge and ε the detector efficiency.

4.1. A brief look at Systematic Errors

Systematic errors (other than scale factors) for a single difference of yields between two in-line cells depend on the relative differences in acceptances $\Delta\mathcal{A}$ and packing fractions Δp_f. Controlling those errors depends, in turn, on the uncertainties in those differences. Control can be accomplished by developing better ways of measuring p_f, and improving the understanding of relative acceptances by carrying out extensive simulations, using optics targets, etc.

The difference of yields from an unpolarized (U) and a longitudinally polarized ($\|$) cell depends on their respective acceptances, lengths ℓ, and the cross sections σ that apply in each case.

$$\Delta Y = \mathcal{A}^U \ell^U \sigma^U - \mathcal{A}^{\|} \ell^{\|} . \sigma^{\|} \tag{3}$$

Using the notation $\ell_A = N_0 z_A (\rho_A / M_A) = N_0 z_A \mathcal{D}_A$, where N_0 represents Avogadro's number, and ρ_A, M_A and z_A are the density, atomic or molecular mass, and thickness of nuclear species A, respectively, the unpolarized and polarized $\ell\sigma$ products are

$$\ell^U \sigma^U = N_0 z \Big(\mathcal{D}_{ND3} (\sigma_N^U + 3\sigma_D^U) p_f^U + \mathcal{D}_{He} \sigma_{He}^U (1 - p_f^U) \Big) \tag{4}$$

$$\ell^{\|} \sigma^{\|} = N_0 z \Big(\mathcal{D}_{ND3} (\sigma_N^U + 3(\sigma_D^U - \frac{Kx}{3} P_{zz} b_1)) p_f^{\|} + \mathcal{D}_{He} \sigma_{He}^U (1 - p_f^{\|}) \Big). \tag{5}$$

Replacing $p_f^{\|} = p_f^U - \Delta p_f$ and $\mathcal{A}^{\|} = \mathcal{A}^U - \Delta\mathcal{A}$, the difference can be written to first order as

$$\frac{\Delta Y}{s\mathcal{A}^U} - f \frac{\Delta p_f}{p_f^U} - \Big(f + \frac{\mathcal{D}_{He}}{\mathcal{D}_{ND3}} \frac{\sigma_{He}^U}{p_f^U} \Big) \frac{\Delta\mathcal{A}}{\mathcal{A}^U} = KxP_{zz}b_1 (1 - \frac{\Delta p_f}{p_f^U} - \frac{\Delta\mathcal{A}}{\mathcal{A}^U}),$$

where $s = N_0 z p_f^U \mathcal{D}_{ND3}$ and $f = \sigma_N + 3\sigma_D - \sigma_{He}(\mathcal{D}_{He}/\mathcal{D}_{ND3})$.

Using this equation, some rough estimates can be made. For a solid angle difference at the limit of the spectrometer angular resolutions $\delta\theta$ and $\delta\phi$, $\partial\Delta\theta = \partial(\theta^U - \theta^{\|}) = \sqrt{2}\delta\theta$ and $\partial\Delta\phi = \sqrt{2}\delta\phi$, the relative difference in acceptances is the relative solid angle error, with

$\partial(\Delta\Omega) = \partial(\Delta\theta\Delta\phi)$. Using the nominal HMS angle resolutions $\delta\theta = \delta\phi = 0.8$ mr the relative error on $\mathcal{A}$ is

$$\frac{\delta\Delta\mathcal{A}}{\mathcal{A}} = \frac{\delta\Delta\Omega}{\Delta\Omega} = \frac{2\delta\theta\delta\phi}{\Delta\Omega} = 5 \times 10^{-4}, \quad (6)$$

where an effective solid angle of 2.5 msr after acceptance matching cuts was used for this estimate (the full HMS solid angle is > 6 msr).

Approximating the nuclear cross sections as multiples of the deuteron cross section, $\sigma_N \simeq 7\sigma_D$, $\sigma_{He} \simeq 2\sigma_D$ so $f \sim 8.5\sigma_D$, the term in eq. (6) proportional to the relative difference of acceptances can then be compared to the r.h.s., which reduces to $P_{zz}b_1/F_1^D$, since $\sigma_D^U = KxF_1^D$. With $\mathcal{D}_{He}/\mathcal{D}_{ND3} = 0.8$, and using conservative values for $P_{zz} = 20\%$ and $p_f = 0.5$, the r.h.s is about 3.3×10^{-3} for $b_1 \sim 0.4 \times 10^{-2}$, as measured by HERMES [12]. The left side is $11.7\Delta\mathcal{A}/\mathcal{A} \sim 6 \times 10^{-3}$. Improvements in P_{zz}, packing fraction, and acceptance matching and resolution can reduce the l.h.s and increase the r.h.s to allow meaningful measurements.

If both cells could polarize the material in opposite tensor polarizations simultaneously, then an extra term appears inside the parenthesis of the r.h.s. of eq. (6), representing the ratio $p = |P_{zz}^+/P_{zz}^-| \simeq 1$ of the polarizations $P_{zz}^{+,-}$ of the upstream and downstream cells ($p = 0$ if only one cell is polarized), so an extra factor of about two would be gained for additional suppression of systematic effects.

To determine the contribution of the packing fraction difference to the systematic errors, we would consider the ammonia mass of about 9 g in the 3 cm long cells at 0.6 packing fraction. Careful weighing of polarizable material loads could resolve 1 mg in about 10 g, keeping this contribution under control. Material preparation in known shapes and dimensions might do even better than that.

In summary: Multiple cell polarized targets are being used and have been used very effectively for controlling systematic uncertainties in experiments with polarized targets, when it's difficult or impossible to flip helicities quickly and frequently, e.g. when using LiD. The in-line configuration favors using a simple solenoidal field for longitudinal spin observables, but transverse observables could still be accessible, at a price. This configuration could be a good option for a program on longitudinal vector and tensor spin observables at JLab. The study of new observables ten to a hundred times smaller than the traditional spin dependent ones requires advanced methods, like the one explored in this report. The potential use of multiple cell targets represents interesting target physics R&D in addition to its compelling physics motivation.

References

[1] Arenhovel H, Leidemann W and Tomusiak E 1988 *Z.Phys.* **A331** 123–138
[2] Leidemann W, Tomusiak E and Arenhovel H 1991 *Phys.Rev.* **C43** 1022–1037
[3] Hoodbhoy P, Jaffe R and Manohar A 1989 *Nucl.Phys.* **B312** 571
[4] Piegaia R N 1988 *UMI-89-17716, fig. 2.8* Ph.D. thesis
[5] Adams D *et al.* (Spin Muon Collaboration) 1999 *Nucl.Instrum.Meth.* **A437** 23–67
[6] `http://wwwcompass.cern.ch/compass/detector/target/Drawings/NH3target07v01.png`
[7] Koivuniemi J 2006 Status of the polarized COMPASS target, talk at Polarized Nucleon Targets for Europe, Rech
[8] `http://wwwcompass.cern.ch/compass/detector/target/Talks/TIS_meet_oct_00.pdf`
[9] Takabayashi N 2002 *CERN-THESIS-2002-051, fig. 5.1* Ph.D. thesis
[10] Richter A 2010 *CERN-THESIS-2010-266, fig. 5.7* Ph.D. thesis
[11] Levorato S 2010 *CERN-THESIS-2008-179, fig 6.4* Ph.D. thesis
[12] Airapetian A *et al.* (HERMES Collaboration) 2005 *Phys.Rev.Lett.* **95** 242001